Optical insight into riverine influences on dissolved and particulate organic carbon in a coastal Arctic lagoon system

Luka Catipovic[1], Luka Catipovic[2], Krista Longnecker[2], Stephen R Okkonen[3], Daniel Koestner[4], and Samuel R Laney[2]

[1]MIT-WHOI Joint Program in Oceanography, Woods Hole, MA, USA
[2]Woods Hole Oceanographic Institution
[3]University of Alaska Fairbanks
[4]University of Bergen

December 7, 2022

Abstract

Optical properties of seawater can provide valuable insight into distributions of dissolved organic carbon (DOC) and particulate organic carbon (POC), provided that their interrelationships are well understood. We examined relationships between DOC and POC, and absorption, backscatter, and fluorescence in a river-fed lagoon system in the coastal Alaskan Arctic during late summer of 2018 and 2019. Over both years analytically measured DOC levels were inversely correlated with salinity (r2 = 0.97) and DOC was positively correlated with dissolved organic material fluorescence (fDOM; r2 = 0.67). However, DOC showed strong correlation with the absorption coefficient at 440 nm (ag(440)) only in 2018 (r2 = 0.95 versus r2 = 0.00056 in 2019). Vertical structure of fDOM in our study area corresponded with density profiles more strongly in 2018 than in 2019, but higher levels of fDOM, ag(440), and backscatter near the bottom in 2019 suggest prior wind-driven mixing or bottom resuspension events. In 2018 and 2019, the spectral slope of the absorption coefficient between 412 and 550 nm was strongly correlated with DOC concentration (r2 = 0.70), and spectral backscattering coefficients were well correlated with POC concentration (r2 = 0.90, 0.71, and 0.59 for 470, 532, and 660 nm respectively). These interannual patterns in the distribution of DOC and POC and their respective relationships with optical proxies likely reflect regional climatological factors such as precipitation over the adjacent watersheds, wind patterns, and residual sea ice in late summer.

Hosted file

`essoar.10512826.1.docx` available at https://authorea.com/users/563933/articles/610991-optical-insight-into-riverine-influences-on-dissolved-and-particulate-organic-carbon-in-a-coastal-arctic-lagoon-system

Optical insight into riverine influences on dissolved and particulate organic carbon in a coastal Arctic lagoon system

L. Catipovic[1, 2, *], K. Longnecker[1], S.R. Okkonen[3], D. Koestner[4], S. R. Laney[1]

[1]Woods Hole Oceanographic Institution, Woods Hole, MA, USA

[2] MIT-WHOI Joint Program in Oceanography, Woods Hole, MA, USA

[3] University of Alaska Fairbanks, AK, USA

[4] University of Bergen, Bergen, Vestland, Norway

[*]Corresponding author: Luka Catipovic (lcatipovic@whoi.edu)

Key Points:

- Absorption, fluorescence, and spectral slope perform well as optical proxies for dissolved organic carbon in Alaskan Arctic coastal waters.
- River discharge appears to be the primary driver of spatial distributions of organic material in Alaskan Arctic coastal waters.
- Backscattering coefficient can serve as a proxy for particular organic carbon concentration in Alaskan Arctic coastal waters.

Abstract

Optical properties of seawater can provide valuable insight into distributions of dissolved organic carbon (DOC) and particulate organic carbon (POC), provided that their interrelationships are well understood. We examined relationships between DOC and POC, and absorption, backscatter, and fluorescence in a river-fed lagoon system in the coastal Alaskan Arctic during late summer of 2018 and 2019. Over both years analytically measured DOC levels were inversely correlated with salinity ($r^2 = 0.97$) and DOC was positively correlated with dissolved organic material fluorescence (fDOM; $r^2 = 0.67$). However, DOC showed strong correlation with the absorption coefficient at 440 nm ($a_g(440)$) only in 2018 ($r^2 = 0.95$ versus $r^2 = 0.00056$ in 2019). Vertical structure of fDOM in our study area corresponded with density profiles more strongly in 2018 than in 2019, but higher levels of fDOM, $a_g(440)$, and backscatter near the bottom in 2019 suggest prior wind-driven mixing or bottom resuspension events. In 2018 and 2019, the spectral slope of the absorption coefficient between 412 and 550 nm was strongly correlated with DOC concentration ($r^2 = 0.70$), and spectral backscattering coefficients were well correlated with POC concentration ($r^2 = 0.90$, 0.71, and 0.59 for 470, 532, and 660 nm respectively). These interannual patterns in the distribution of DOC and POC and their respective relationships with optical proxies likely reflect regional climatological factors such as precipitation over the adjacent watersheds, wind patterns, and residual sea ice in late summer.

0. Plain language summary

When light interacts with seawater, it can either be absorbed or scattered by the contents of the water. The degree to which these processes occur offers valuable insight into the chemical and physical properties of seawater. These quantities, known as the inherent optical properties (IOPs) of the water, can be studied to better understand carbon composition and concentration in complex aquatic systems such as Arctic lagoons and estuaries. However, in order to use these IOPs as proxies to study carbon biogeochemistry, we must first understand the relationships between said optical properties and carbon characteristics. This study presents analytically measured concentrations of dissolved and particulate organic carbon in surface waters within Stefansson Sound, AK, a coastal Arctic lagoon. We then use these measurements to investigate the relationships between organic carbon and the optical properties of the waters in this region. We found that across two years these relationships are robust and can facilitate understanding of carbon characteristics in lieu of direct measurement. Finally, we determine that the amount of dissolved organic carbon found in the surface waters of this region is controlled by the precipitation over the adjacent watersheds, which increases the river flow and carbon delivery into the coastal margin.

1. Introduction

Optical properties of seawater are often used to examine facets of marine organic carbon in complex coastal waters (Osburn et al., 2016; Reynolds et al., 2016). As proxies, these optical properties are well suited for studying biogeochemical parameters such as organic carbon quality, distribution, source, and concentration at higher spatial and temporal scales, compared to current approaches involving analysis on discrete water samples (Dickey & Chang, 2001). The fluorescence of dissolved organic material (fDOM), the spectral absorption coefficient of the dissolved material ($a_g(\lambda)$), and the optical backscattering coefficient ($b_b(\lambda)$) have all been shown to positively correlate with the concentration of organic matter as well as serve as indicators of its source and composition (Gonçalves-Araujo et al., 2016; Matsuoka et al., 2011; Reynolds et al., 2016). Instruments that measure optical backscatter and fluorescence have been autonomously deployed in timeseries studies to examine the timing and magnitude of seasonal events in Arctic environments (Laney et al., 2022). Understanding more about the optical signatures of organic material in complex Arctic coastal systems can further improve our capacity to study these waters in a larger context. Such optical relationships have significant potential for improving our understanding of carbon cycle dynamics, but before these techniques can be implemented autonomously it is essential to define the relationships between analytical measurements of organic material concentration and optical proxies.

Coastal Arctic lagoons and estuaries similar to Stefansson Sound are poorly understood in this respect, not only in terms of these optical relationships, but also with respect to areal and vertical distributions of organic material as well as the interannual variability driven by large-scale climatological trends. The system is further complicated by the presence of sea ice, seasonal

events such as the spring freshet, and any local rivers that effuse organic material into the coastal margins (Matsuoka et al., 2012; Stedmon et al., 2011). The snow cover and active layer across each river's watershed begins to thaw in late May resulting in a rapid increase in fluvial discharge. This event often accounts for more than 50 % of the annual freshwater input into the coastal margins (McClelland et al., 2014). Throughout the summer months the rivers continue to supply terrigenous material to the lagoons and estuaries, but this is not the only source of freshwater and organic nutrients to these regions. As the Arctic warms, ice transported from the Canadian Basin through the Beaufort Sea is comprised of an increasing proportion of younger ice (Howell et al., 2016). This younger, often first-year ice, is more likely to break off from the pack and drift shoreward. Melting first year ice in the coastal margins provides a new source of fresh water and organic material to the surface ocean which is not fully quantified in terms of the amount of material delivered or qualified in terms of its chemical character (Underwood et al., 2019). Moreover, the sea-ice makes direct sampling logistically challenging as ice floes can block access to desired research areas further heightening the need for *in situ* optical infrastructure to increase research capacity. The hurdles associated with interannual variability, along with the already complex intricacies of these coastal estuaries require a systems level approach to adequately describe the spatial characteristics of organic and optical properties. Precipitation, winds, currents, and tides all have profound impacts on the day-to-day water structure, thus this research relies on the culmination of understanding climatology, terrestrial hydrography, and regional seasonality. Moreover, a multitude of techniques from aspects of physical oceanography, chemical oceanography, and ocean optics must be employed to capture these structural dynamics.

The objective of this current study was to quantify the relationships between organic carbon and fluorescence, absorption, and optical backscatter in the surface waters of coastal Arctic estuaries during late summer. We addressed this in a two-year field study in a coastal Arctic lagoon system (Stefansson Sound, AK) along the Beaufort shelf (Arctic Ocean). This system is partially enclosed by barrier islands 10-15 km offshore and is fed by the Sagavanirktok and Kuparuk Rivers. Stefansson Sound experiences seasonal landfast ice coverage, lingering first-year sea ice, riverine injection, high winds, and turbid waters. All together, these complexities make for a diverse system that has the potential to offer insight into other coastal Arctic estuaries that also experience some or all of these features. In this study, we first describe relationships between optical proxies and analytically measured dissolved organic carbon (DOC) and particulate organic carbon (POC) concentrations and assess their efficacy for estimating characteristics associated with source and composition. Second, we present vertical profiles of absorption, fDOM, backscatter, and transmittance to examine the areal and vertical distribution of freshwater in Stefansson Sound and how said distribution varies year-to-year with respect to terrestrial drivers. Finally, we discuss each year's physical environmental characteristics and how their fundamental differences affect the aforementioned optical relationships and annual variability.

2. Methods

2.1. Study area

Distributions of DOC and POC, along with the absorption coefficient of dissolved material at 440 nm ($a_g(440)$), total backscattering coefficients at 470 nm, 532 nm, and 660 nm ($b_b(470)$, $b_b(532)$, $b_b(660)$), fluorescence of dissolved organic material (fDOM), temperature, and salinity were measured in Stefansson Sound, AK in late summer of 2018 (6 – 10 September) and 2019 (9 – 13 August). Stefansson Sound is a shallow lagoon system partially enclosed by barrier islands

along the Beaufort Shelf that receives input from two principal rivers with deltas 30 km apart, the Sagavanirktok River (14300 km^2 drainage area) and the Kuparuk River (8100 km^2 drainage area), along with several smaller rivers including the Shaviovik River (4028 km^2 drainage area) and the Kadleroshilik River (1290 km^2 drainage area). These rivers all drain tundra overlain watersheds with the Sagavanirktok and, to a lesser extent, the Shaviovik also draining mountainous regions of the Brooks Range at their headwaters south of the coastline (**Fig. 1**).

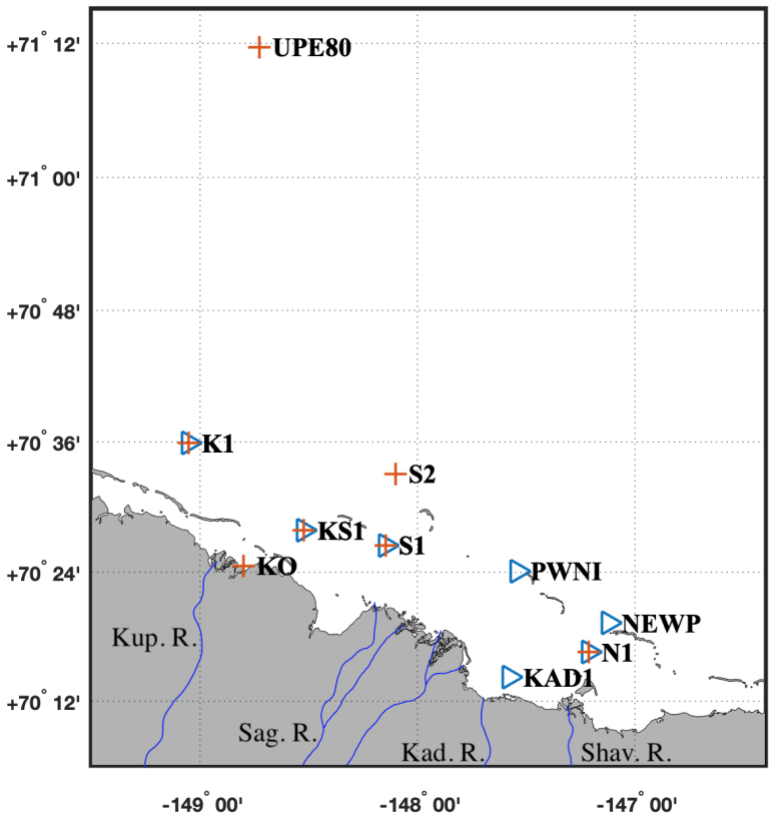

Figure 1. Sample locations for the September 2018 field season (blue triangles) and August 2019 field season (orange crosses). Overlap indicates repeat sampling in both years.

Samples were collected across ten locations (**Fig. 1**) within the study area, arranged to encompass the coastal lagoon receiving input from the mouths of the two principal rivers. In 2018, sampling was restricted to inshore locations to respect the local whaling operations. In

2019, sampling covered a similar inshore region but with the addition of three other stations not visited in 2018: one at the mouth of the Kuparuk River delta (KO), one just outside the barrier islands north of the mouth of the Sagavanirktok River (S2), and one at the shelf break ~ 60 km offshore directly north of the mouth of the Kuparuk River (UPE80). These stations were chosen to represent riverine and oceanic endmembers, respectively.

2.2 Discrete sampling of DOC and POC

Samples for dissolved and particulate analysis were collected from the depths listed in **Table 1** using 5 L Niskin bottles. The bottom depth at the Kuparuk River mouth was < 2 m and thus only surface samples were taken from there (station KO in **Fig 1**.). Samples were filtered through combusted Whatman glass fiber filters (GF/F; nominal pore size 0.7 μm) then acidified to pH 2 with 12 M HCl and stored at 4 °C until processed at the Woods Hole Oceanographic Institution on a Shimadzu TOC-V_{CSH} total organic carbon analyzer. Reported DOC data are the average of triplicate samples taken at each depth except for at N1 in 2018 and KO in 2019 from which there are only two replicates. Across all samples, the coefficients of variation of replicates were on average 1.6 % in 2018 and 3.9 % in 2019. Measurements were made using potassium hydrogen phthalate as a standard solution. DOC concentration was determined by subtracting the instrument blank area from the average peak area and dividing by the slope of the standard curve. Comparisons to low carbon water and deep-sea reference water provided by Prof. D. Hansell (University of Miami) were made daily.

For the analysis of POC concentration, approximately 100–1400 mL of seawater were filtered through 25 mm diameter GF/F filters at low vacuum (< 120 mm Hg) using pre-combusted filters.

Filters with retained particles were dried in a small oven at about 55 ºC and stored for laboratory-based analysis. Elemental carbon analysis of POC filters was performed at the University of California Santa Barbara Marine Science Institute Analytical Laboratory following standard methodology (Parsons et al., 1984). Blank filters were prepared utilizing approximately 50 mL of GF/F filtered seawater collected from several stations to adjust POC estimates for adsorption of dissolved organic carbon onto the filters as well as other sources of contamination (Novak et al., 2018). These corrections resulted in an average reduction of 11% for POC. Duplicate filters were collected, and results were typically averaged to determine a final estimate of POC at each station's sampling depths. Coefficients of variation between replicates of POC were on average 7%.

2.3 Watershed and river characteristics

Volumetric discharges were provided by USGS stream gauges that monitored the Kuparuk River (USGS 15896000, located 9 km upstream from the river mouth) and the Sagavanirktok River (USGS 15908000, located roughly 90 km upstream from the river mouth). Volumetric discharge from the stream gauges is reported every 15 minutes. Precipitation data from the University of Alaska at Fairbanks Toolik field station (68.63 N, 149.60 W), 200 km south of the coast, were used representatively as a metric of rainfall over the watersheds of the rivers. These data were collected using a tipping bucket rain gauge (Texas Electronics TE525WS) (EDCT, 2020; Youcha et al., 2015). Precipitation is reported in this study as a 24-hour running mean. Cumulative precipitation reported in the week prior to each sampling period was estimated by calculating the area under the running mean using the trapezoid method.

227 **2.4 Hydrographic and optical properties of vertical profiles**

228 Water column structure was measured at each station using a custom profiling package, the
229 instruments on this package (~1 m high) were separated at maximum by ~ 0.5 m and vertical
230 offsets were corrected for during post-processing. The sensor suite included hydrographic and
231 optical sensors: a conductivity, temperature, and depth meter (SBE-49 FastCAT), a spectral
232 absorption and attenuation meter (WETLabs ac-s), a three-channel active sensor (WETLabs
233 FLBBCD) which measured fluorescence of dissolved organic matter (fDOM), and a three-
234 wavelength volume scattering function sensor (WETLabs VSF3). The VSF3 measures the
235 volume scattering function (β) at scattering angles of 100º, 125º, and 150º for light wavelengths
236 of 470 nm, 532 nm, and 660 nm. Backscattering coefficients for each light wavelength were
237 calculated following standard methods recommended by WETLabs. In brief, this involved
238 converting the measured β values to polar steradian area, fitting a 3rd order polynomial to the
239 new values with an added fourth point (sin (π radians) = 0), and integrating under the polynomial
240 fit function from π/2 to π. This method results in a maximum 1 % error when tested against
241 published volume scattering functions (Petzold, 1972). The WETLabs FLBBCD measures
242 fDOM fluorescence of 460 nm light with an excitation wavelength of 370 nm (370/460 nm)
243 which was chosen to align with the expected fluorescence of terrestrial humic material
244 anticipated to be injected by the rivers into the coastal margin.
245
246 To provide optical information on the dissolved constituents, the package was deployed twice at
247 each station, with one deployment utilizing a 0.2 μm capsule filter (Whatman POLYCAP AS)
248 placed on the inlet of the ac-s pump. These ac-s data were processed by WETLabs proprietary
249 software to engineering units and then further corrected for temperature and salinity in

MATLAB 2021a (Sullivan et al., 2006). Spectral slopes of absorption between 412 nm and 550 nm ($S_{412\text{-}550}$) were calculated using a single exponential model fit of corrected spectra. Profiles were taken in series of two at every station in each year. During the first cast, the ac-s was fitted with capsule filters and allowed to measure absorption of the dissolved constituents. The cast was also set to rest for 5 minutes at the near-surface and near-bottom depths to allow ample time for collecting statistically significant optical data where discrete water samples were retrieved for DOC and POC analysis. The data from these casts were used in the optical regressions against DOC and POC. During the second casts, the ac-s was not fitted with cartridge filters to examine the total absorption including particles. Each other instrument was setup the same way for each cast. Finally for the creation of the profiles for display purposes, the upcast was used to capture data in the top two meters of the water column. Mixed-layer depths were determined according to the most relevant maximum Brunt-Vaisala frequency peak in each profile. Mixed layers depths were defined as the first peak below the peak associated with the freshwater lens which was generally in the first 2 m of the water column (**Fig. S1 & S2**).

2.5 Statistical Analyses

Model-II geometric mean linear regression analyses were performed to determine the strength of any relationships between various optical proxies (independent variable) and DOC or POC (dependent variable). Regression models were evaluated for accuracy using two common metrics: root mean square deviation (RMSD) and median absolute percent difference (MdAPD). The RMSD assesses model accuracy in absolute units by quantifying the mean of the squared residuals between the observed and the model-predicted values and thus can be susceptible to outliers. The MdAPD is less sensitive to large errors by utilizing the median of the absolute

273 difference between model-predicted and observed values normalized by observed values and
274 provides a standard metric for model assessment as a percentage.
275
276 **3. Results**
277 **3.1 Spatial distribution of organic matter in Stefansson Sound**
278 In 2018, DOC concentrations ranged from 92.1 to 310 μM at the surface and 83.1 to 127 μM
279 near the bottom. In this same year POC values ranged from 0.133 to 0.502 g m^{-3} at the surface
280 and 0.100 to 0.160 g m^{-3} near the bottom. In 2019, we observed a range of DOC concentrations
281 from 80.1 to 127 μM at the surface and 78.1 to 87.5 μM near the bottom; POC values ranged
282 from 0.156 to 0.509 g m^{-3} at the surface and 0.070 to 0.536 g m^{-3} near the bottom. The fraction of
283 dissolved organic carbon to total organic carbon (DOC/(DOC+POC)) was above 0.85 for all
284 samples in 2018 and ranged from 0.65 to 0.93 in 2019 (**Table 1**). In 2018, higher DOC
285 concentrations were observed at the eastern stations (PWNI, N1, NEWP, KAD1) than at the
286 western stations (K1, KS1, S1; unpaired *t*-test, $p = 0.138$). In 2019 DOC concentrations were
287 more uniform across all stations. The difference between surface and bottom DOC
288 concentrations was significantly higher in 2018 than in 2019 (unpaired *t*-test, $p < 0.05$). In 2019,
289 the DOC concentrations are generally similar to that found at the offshore UPE80 station
290 suggesting a high proportionate presence of offshore water in the inshore coastal margin, and a
291 well-mixed water column. Surface POC concentrations were significantly higher than bottom
292 concentrations in 2018 (unpaired *t*-test, $p < 0.05$) while concentrations measured in 2019
293 exhibited no significant areal or vertical differences.

Table 1. DOC and POC concentrations and fraction dissolved (DOC/TOC, where TOC is DOC + POC) at the surface and bottom from both field seasons. DOC is reported in units of micromolar, POC

is reported in units of g m-3 and the conversion to micromolar takes the form: $\frac{1\ g\ C}{1\ m^3} \times \frac{1e6\ \mu g\ C}{1\ g\ C} \times \frac{1\ m^3}{1000\ L} \times \frac{1\ \mu mol\ C}{12.01 \mu\ g\ C}[=]\frac{\mu mol\ C}{L}$*. DOC/TOC ratio is unitless. Reported errors are standard deviation within a triplicate or duplicate set of samples unless the error is zero in which case only one replicate was available.*

		2018		2019	
Station	**Property**	**Surface**	**Bottom**	**Surface**	**Bottom**
KO	Sample depth	~	~	0.6	~
	DOC	~	~	126 ± 0.8	~
	POC	~	~	0.388 ± 0.011	~
	DOC/TOC	~	~	0.80 ± 0.01	~
K1	Sample depth	1.1	13.6	2.0	17.3
	DOC	92.1 ± 4.1	83.1 ± 1.87	83.0 ± 5.06	79.7 ± 0.99
	POC	0.202 ± 0.005	0.115 ± 0.000	0.156 ± 0.047	0.335 ± 0.013
	DOC/TOC	0.85 ± 0.06	0.90 ± 0.03	0.86 ± 0.09	0.74 ± 0.02
KS1	Sample depth	1.5	6.1	1.5	6.4
	DOC	148 ± 1.34	116 ± 3.30	107 ± 0.73	81.5 ± 7.36
	POC	0.133 ± 0.018	0.134 ± 0.009	0.366 ± 0.045	0.189 ± 0.037
	DOC/TOC	0.93 ± 0.01	0.91 ± 0.04	0.78 ± 0.02	0.84 ± 0.12
S1	Sampled depth	1.1	5.7	1.7	6.5
	DOC	159 ± 4.3	117 ± 0.87	86.9 ± 8.0	87.5 ± 6.02
	POC	0.502 ± 0.024	0.159 ± 0.003	0.509 ± 0.078	0.493 ± 0.065
	DOC/TOC	0.79 ± 0.04	0.90 ± 0.01	0.67 ± 0.12	0.68 ± 0.09
S2	Sample depth	~	~	1.4	17.0
	DOC	~	~	80.1 ± 1.81	81.3 ± 0.98
	POC	~	~	0.158 ± 0.010	0.181 ± 0.032
	DOC/TOC	~	~	0.86 ± 0.03	0.84 ± 0.03
PWNI	Sample depth	1.3	6.2	~	~
	DOC	153 ± 0.76	108 ± 1.43	~	~
	POC	0.234 ± 0.00	0.104 ± 0.00	~	~
	DOC/TOC	0.89 ± 0.01	0.93 ± 0.02	~	~
KAD1	Sample depth	1.1	4.7	~	~
	DOC	223 ± 0.79	145 ± 2.83	~	~
	POC	0.242 ± 0.00	0.146 ± 0.00	~	~
	DOC/TOC	0.92 ± 0.00	0.92 ± 0.03	~	~
NEWP	Sample depth	1.4	6.6	~	~
	DOC	168 ± 1.27	109 ± 0.83	~	~
	POC	0.248 ± 0.001	0.100 ± 0.000	~	~
	DOC/TOC	0.89 ± 0.01	0.93 ± 0.01	~	~
N1	Sample depth	1.3	6.0	1.4	5.2
	DOC	310 ± 4.50	127 ± 1.42	84.8 ± 5.43	82.4 ± 7.14
	POC	0.310 ± 0.026	0.160 ± 0.014	0.291 ± 0.044	0.536 ± 0.072
	DOC/TOC	0.92 ± 0.02	0.90 ± 0.02	0.78 ± 0.08	0.65 ± 0.10
UPE80	Sample depth	~	~	2.3	47.50
	DOC	~	~	87.1 ± 1.50	78.1 ± 1.65

POC	~	~	0.181 ± 0.034	0.070 ± 0.016
DOC/TOC	~	~	0.85 ± 0.02	0.93 ± 0.03

294

295

296 **3.2 Relationships between optical properties and organic matter**

297 Over both years, we observed positively correlated relationships between optical variables
298 fDOM, $a_g(440)$, and $S_{412\text{-}550}$, and DOC (**Fig. 2**). The correlation between fDOM and DOC was
299 strong ($r^2 = 0.67$), however the strength of the regression is heavily weighted by the 2018
300 relationship between the two variables ($r^2 = 0.94$) as we observed significantly higher surface
301 DOC concentrations than were seen in 2019 (**Table 1**; unpaired *t*-test, $p < 0.05$). The regression
302 was weak in 2019 ($r^2 = 0.29$) which brought the overall correlation down across both years (**Fig.**
303 **2a)**. The value of the regression model at the ordinate suggests that 29.4 µM of the DOC pool
304 does not fluoresce at the 370 nm excitation wavelength used by our fluorometer (WETLabs
305 FLBBCD).

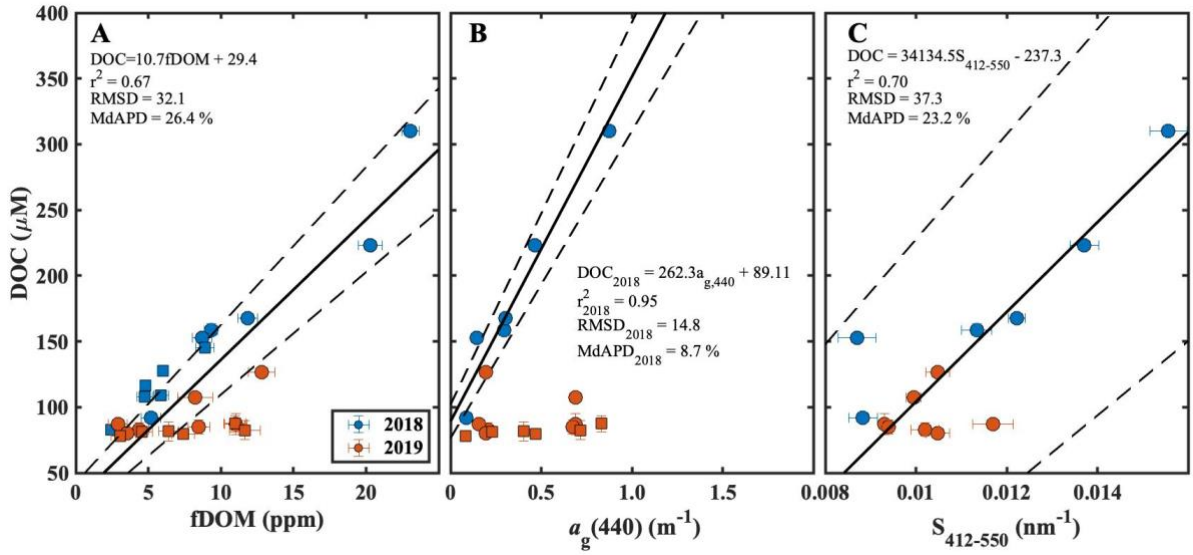

Figure 2. Linear regressions between DOC and optical variables across both years: a) fDOM (370 nm/ 460 nm), b) $a_g(440)$, and c) $S_{412\text{-}550}$. Symbols indicate surface samples (circles) and

samples collected below the mixed layer (squares, not included in regressions). Dotted lines indicate ± SD.

306

307 The concentration of DOC correlated strongly with $a_g(440)$ in 2018 ($r^2 = 0.95$), and very weakly
308 in 2019 ($r^2 = 0.00056$) (**Fig. 2b**). Extrapolating the 2018 regression to the ordinate suggests 89.1
309 µM of DOC does not absorb 440 nm light which is nearly three times the concentration that does
310 not fluoresce at 370 nm as stated above. The spectral slope between 412 nm and 550 nm ($S_{412-550}$)
311 correlated well with DOC concentration across both years ($r^2 = 0.71$) indicating an increase
312 in DOC with increasing $S_{412-550}$ (**Fig. 2c)**. The negative value at the regression ordinate suggests
313 that there is no concentration of DOC that would be described by a spectral slope of zero
314 between these wavelengths, although the uncertainty bounds of this regression are quite large.

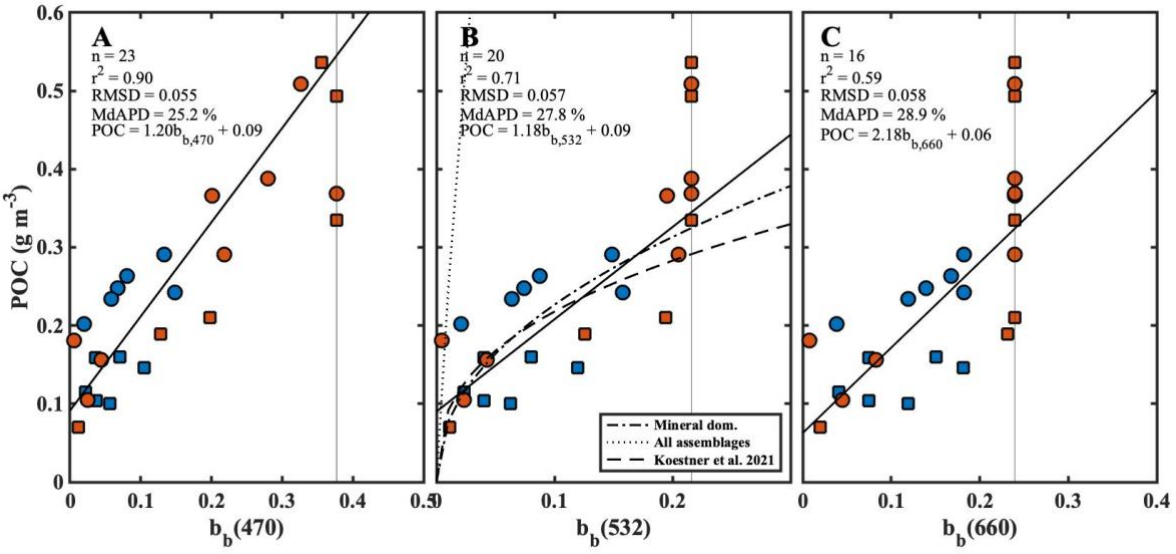

Figure 3. POC vs. backscattering of a) 470 nm, b) 532 nm, and c) 660 nm light. Panel b includes regression lines showing relationships between POC and $b_b(550)$ in mineral dominated assemblages and all assemblages from Reynolds et al. (2016), and a relationship between POC and $b_b(552)$ measured by a LISST-VSF in Stefansson Sound from Koestner et al.

(2021). Data lying on the vertical lines in each panel are at sensor maximum and are not included in the regressions. The colors and shapes of the symbols are as described in figure 2.

Correlations between POC concentration and all wavelengths of optical backscatter measured were strong ($r^2 = 0.90$, $r^2 = 0.71$, and $r^2 = 0.59$ for 470 nm, 532 nm, and 660 nm, respectively) **(Fig. 3).** The sensor maximum for the instrument used (WETLabs VSF3) was highest when measuring $b_b(470)$ and lowest when measuring $b_b(660)$ resulting in the inclusion of more data points in the POC vs. $b_b(470)$ relationship (n = 23) and less in the relationships with $b_b(532)$ and $b_b(660)$ (n = 20 and n = 16, respectively).

The regression line for POC and $b_b(532)$ falls within relationships found in other studies representative of mineral-dominated particulate assemblages and assemblages inclusive of inorganic and organic particulates (Koestner et al., 2021; Reynolds et al., 2016). The regression-model derived by Koestner et al. (2021) was determined from POC samples taken from the same cruises in the current study but using a different scattering meter (LISST-VSF, Sequoia Scientific). Additional analysis described in Koestner et al. (2021) revealed that the particulate assemblages were primarily inorganic-dominated.

3.3 Physical and optical vertical structure

The vertical structure of water column density (**Fig. 4, left column**) in both years indicates a freshwater source to the surface waters. In 2018, density profiles tend to have at least two distinct layers with weak stratification throughout the water column. This is seen in every station except KS1 which lies west of the Sagavanirktok River. Station K1 also lies west of the Sagavanirktok

River but was covered by an ice floe and the profiles at this location show multiple strata formed by the melting of this ice, along with riverine injection (**Fig. 4**). The vertical structure measured in 2019 displays stronger stratification with a thinner freshwater layer at the surface less than 2 m thick. At the stations with deeper bottom depths (K1, S2, and UPE80) a defined mixed-layer exists over an oceanic layer, but the transition is found much lower at ~4 m, ~8 m, and ~19 m, respectively. In both years, at least to some extent, the density structure is manifested in the shape of optical profiles.

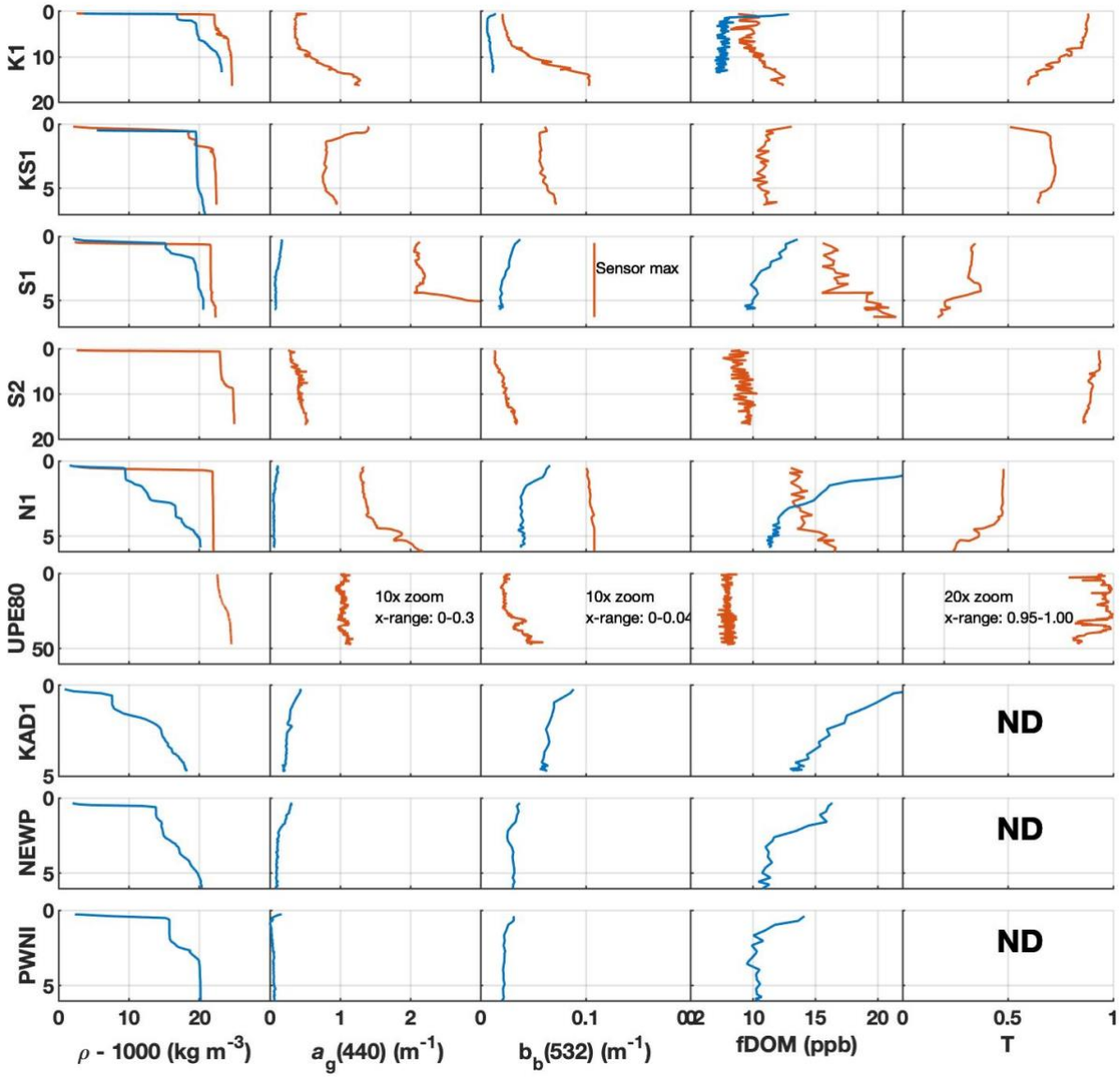

Figure 4. Vertical profiles from each station of density of seawater (ρ), $a_g(440)$, $b_b(532)$, *fDOM, and beam transmittance (T). 2018 profiles are shown in blue and 2019 profiles are shown in orange. ND indicates transmittance data were not collected at selected stations in 2018.*

343

344 The 2018 optical profiles of $a_g(440)$, $b_b(532)$, and fDOM loosely mirror density profiles with
345 profiles of each optical proxy showing higher values near the surface than near the bottom (**Fig.**
346 **4**). At most stations in 2018 lower density water contains elevated levels of fDOM and $b_b(532)$
347 correlating with elevated levels of DOC and POC (**Fig. 2 and Fig. 3**) which is expected in water
348 of terrigenous origin. However, at K1 in 2018, $b_b(532)$ is lower just below the surface and
349 increases with depth while fDOM is elevated at the surface and nearly constant with increasing
350 depth. Thus, the ice floes found atop and surrounding this station are potentially supplying a
351 source of fluorescent DOC without any accompanying POC. While this is not necessarily seen in
352 the discrete measurements, it is possible the analytical samples were taken from below this
353 phenomenon. In 2019, $a_g(440)$, $b_b(532)$, and fDOM are generally highest near the bottom with
354 constant values near the top and mid water column. The water column at UPE80 is relatively
355 optically clear in terms of $a_g(440)$, $b_b(532)$, and fDOM, but there are noted increases in value of
356 each proxy just below the mixed layer.

357

358 **3.4 Stefansson Sound: hydrography, hydrology, and wind**

359 We saw clear separation in surface temperature and salinity between both years despite returning
360 to three of the same stations in year two of our study. In 2018, mean surface salinity across all
361 stations within the coastal margin was 13.9 PSU while in 2019 mean surface salinity in the same

region was significantly different at 26.8 PSU (unpaired *t*-test, $p < 0.05$). The mean surface temperature was 2.3 ºC in 2018 and 5.7 ºC in 2019 (unpaired *t*-test, $p < 0.05$) (**Fig. 5)**. The salinity of the ambient water covering the shelf has been observed to vary from 20 - 35 PSU annually with fresher values during the summer months when the rivers are running, while water temperatures range from -1.6 °C to -1.8 °C during winter and increase to as high as 8 °C in this study during August 2019 (Weingartner et al., 2001). The separation in temperature-salinity space between the two years is likely attributed to changes in riverine injection as well as the presence of sea ice meltwater in 2018 and wind-driven mixing.

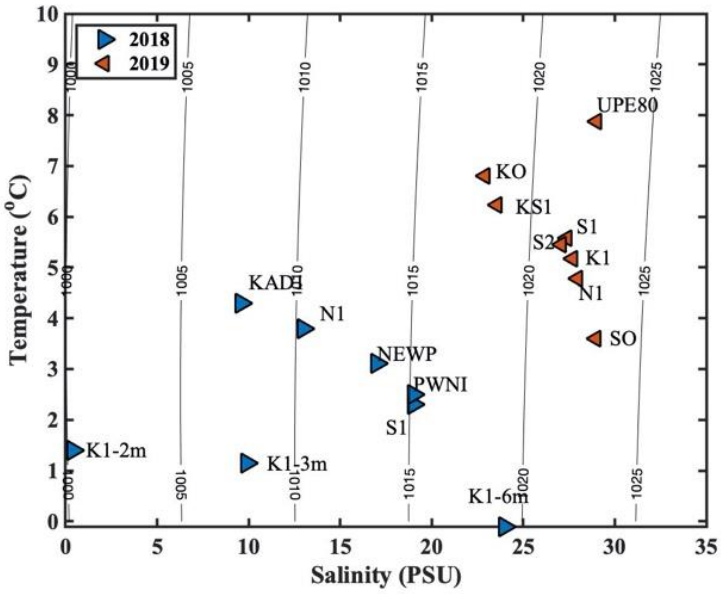

Figure 5. Temperature and salinity relationships for all surface samples collected across both field seasons. Lines indicate contours of constant density in units of kg m^{-3}. In 2018, Station K1 was covered by an ice-floe and had multiple strata near the surface.

Year-to-year differences in vertical density structures also likely reflect year-to-year differences in river waters discharged into the coastal margin in each year. In the week prior to the 2018

372 sampling effort, 50 % more accumulated precipitation was recorded at Toolik Field station than
373 in the week prior to the 2019 sampling effort. This increase in precipitation is reflected by a 66
374 % increase in cumulative volumetric discharge in the 1 – 10 September 2018 period over the 4 –
375 13 August 2019 period (**Fig. 6**). Moreover, the USGS Sagavanirktok stream gauge near pump
376 station 3 recorded river water temperatures of ~ 4 ºC in 2018 and ~8 ºC in 2019 during each
377 respective sample period, which in turn is reflected by cooler and fresher surface waters in the
378 coastal margin in 2018 (**Fig. 5**).

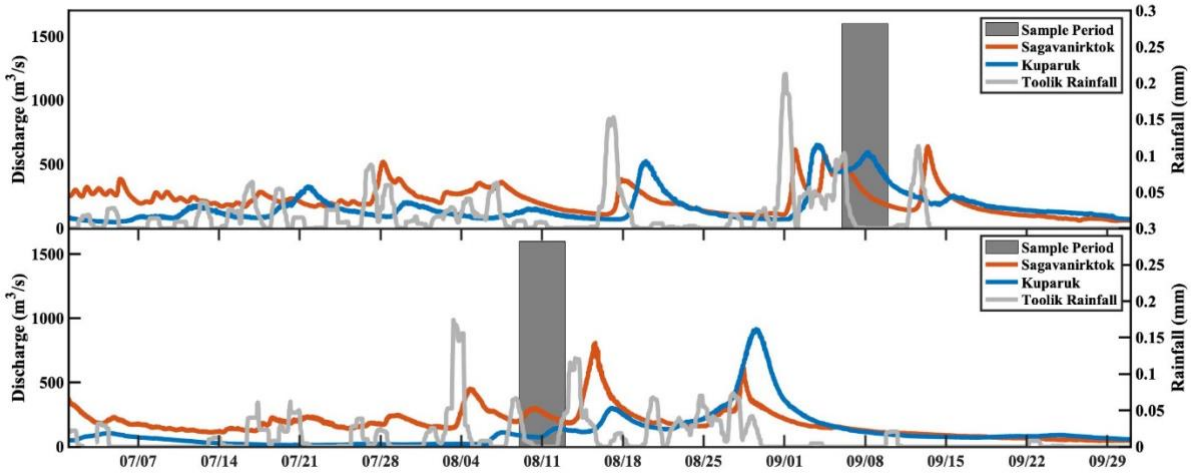

Figure 6. 1018 (top panel) and 2019 (bottom panel) volumetric flow measured at stations USGS 15896000 and USGS 15908000 for the Kuparuk and Sagavanirktok, respectively. Rainfall data were measured at Toolik Field Station and are presented as a 24-hour running mean (EDCT, 2020). Our field studies occurred between 6 - 10 September 2018 and 9 - 13 August 2019 (shaded areas).

379 With the constant source of freshwater from the rivers, it is expected that this mechanism would
380 also be the primary source of organic matter to the coastal system. Over both years, DOC
381 concentration decreases with increasing salinity ($r^2 = 0.97$) indicating that DOC is primarily
382 delivered within the plumes of fresh river water or by melting sea ice. Extrapolating this

383 relationship to the ordinate reveals that incoming freshwater contains a DOC concentration of
384 319.8 μM (**Fig. 7**). This value falls in the middle of the 100 – 600 μM range measured in the
385 Sagavanirktok and Kuparuk Rivers in other studies during late summer (McClelland et al.,
386 2014). Inclusion of the N1 station in the regression reduces the regression coefficient ($r^2 = 0.83$)
387 while raising the y-intercept to 429.6 μM, which is still within the range found in the literature.

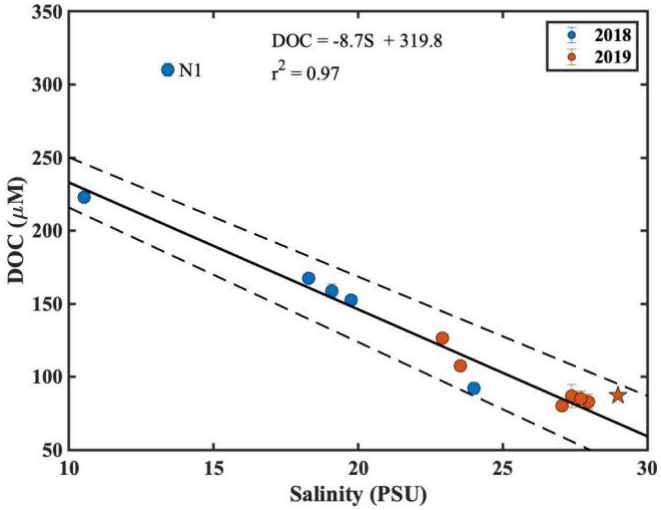

Figure 7. Relationship between surface DOC concentration and salinity within Stefansson Sound over both years. Dotted lines indicate ± 1 SD. Star symbol indicates the marine end member station (UPE80).

388

389 Hydrographic, biogeochemical, and optical properties at a given location are also affected by
390 whether the winds blow from the east or the west. Westerly winds push water against the coast
391 and facilitate a river plume that spreads tightly along the coast towards the east. Easterly winds
392 push against the Coriolis driven plume motion and create a more bulbous river plume and
393 facilitate wind-driven mixing in the water column. In 2018, prevailing winds blew from the west
394 while in 2019 prevailing winds tended to blow from the east **(Fig. S3**). These Ekman dynamics

395 are partially responsible for the areal distribution of river plume water and thus play a large role
396 in influencing temperature, salinity, DOC, and POC characteristics at a given station.
397
398 **4. Discussion:**
399 This study explores optical and chemical relationships in Stefansson Sound over two adjacent
400 years in the late summer open water season. We found strong correlations between common
401 optical proxies and analytically measured DOC and POC despite there being complex
402 differences in the hydrology and hydrography in the coastal margin between the two years.
403 Various physical phenomena (e.g. wind velocity, rainfall over the terrestrial watersheds, and the
404 presence of sea ice) influence the optical complexity of coastal waters in this region. These
405 findings describe how these physical properties affect the relationships between optical proxies
406 and organic material in a coastal Arctic lagoon system
407
408 The data presented here provide three primary contributions to the greater understanding of
409 Alaskan coastal Arctic margins receiving riverine input throughout the year. First, the data
410 presented here represent observations of both analytically measured DOC and POC as well as
411 their corresponding *in situ* optical proxies in a coastal polar region during two environmentally-
412 different summer seasons: the 2018 sample period was characterized by increased precipitation,
413 persistent westerly winds, and lingering sea ice in late summer, while 2019 was much warmer
414 than average in the months prior to sampling. Second, this study shows that measured optical
415 proxies in Stefansson Sound are significantly-correlated with the composition and concentration
416 of DOC and POC thereby offering insight into the biogeochemical relationships between organic
417 material and ocean optics. Third, we found that across the two years, the spatial distributions of

418 temperature, salinity, and organic material were influenced by riverine discharge, as well as wind
419 driven mixing. The late-summer discharge into the coastal margin appears to be controlled by
420 precipitation rates over the feeding watersheds of each of the rivers. The relationships found in
421 this study provide quantitative infrastructure to support further autonomous *in situ* measurements
422 to capture temporal dynamics. Together, these findings provide novel insight into how physical
423 phenomena such as precipitation and wind affect the structure of biogeochemical and optical
424 variables throughout the coastal Arctic water column.
425
426 **4.1 Optical proxies for DOC and POC in Stefansson Sound**
427 The primary findings in this study are the relationships between DOC and fDOM, $a_g(440)$, and
428 $S_{412\text{-}550}$ as well as the relationship between POC and optical backscatter at light wavelengths 470
429 nm, 532 nm, and 660 nm. The strongest relationships for optical proxies across both years were
430 between fDOM and DOC ($r^2 = 0.67$) and $b_b(470)$ and POC ($r^2 = 0.90$). The weaker relationships
431 were between $a_g(440)$ and DOC in 2019 ($r^2 = 0.00056$) and $b_b(660)$ and POC ($r^2 = 0.59$) using
432 data from 2018 and 2019. DOC and fDOM were well-correlated in 2018 ($r^2 = 0.94$) but not as
433 well in 2019 ($r^2 = 0.29$); we attribute this to compositional differences in the bulk DOC pool
434 between the two years. The fluorometer (WETLabs FLBBCD) used in this study was tuned to an
435 excitation-emission pair resemblant of Coble peak C (ex = 350 nm/ em = 420-480 nm) which is
436 representative of the presence of lignin phenols and terrestrial humic materials (Coble, 1996;
437 Walker et al., 2013). However, in our 2019 study we observed a dynamic range of fDOM
438 concentrations from 2 to 14 ppm across all stations without a statistically significant
439 corresponding change in DOC concentration. This finding suggests that the DOC pool in 2019
440 may have been composed of organic material that does not fluoresce or fluoresces at a different

441 excitation-emission combination. Coble peak A (ex = 260/ em = 380-460) is also commonly
442 found in the source waters of this region and represents a fluorescent pool within the bulk DOC
443 that would not be triggered by fluorometer used in this study (Ward et al., 2015). Peak M, which
444 indicates the presence of marine humic material, is also detected by a separate fluorescence pair
445 (ex = 380 nm/ em = 420 nm). Shifts in the relative contributions by these three groups may show
446 variability within the single pair fDOM signal, but not within the analytical techniques used to
447 measure bulk DOC concentration.
448
449 Considering these caveats, optical proxies for estimating DOC can still achieve accuracy as high
450 as about 25% in terms of MdAPD and could provide an avenue for collecting data with higher
451 temporal resolution using *in situ* instrumentation fixed to autonomous platforms in this coastal
452 region. Specifically, fluorometers can be successfully implemented in autonomous sampling
453 platforms to obtain a high temporal resolution understanding of drivers of carbon injection in this
454 region such as freshet timing and precipitation events. This has been proven to work both in open
455 water and below full thickness icepack for periods of up to a year (Laney et al., 2022). However,
456 our study shows that fluorometers may be best used in pairs or trios due to the existence of
457 multiple organic fluorophores within the bulk carbon pool.
458
459 The dissolved absorption coefficient at 350 nm is a common proxy used in literature to
460 approximate DOC concentration (Mann et al., 2016; Spencer et al., 2012). This is due to the high
461 concentration of aromatic and conjugated material that absorbs heavily in the UV within bulk
462 DOM pools (Weishaar et al., 2003). This study shows that these correlations hold into the blue
463 region of the visible spectra as well, demonstrating a strong relationship between DOC and the

absorption coefficient at 440 nm ($r^2 = 0.95$ in 2018) and suggesting a dominant presence of terrestrially derived organic material as is consistent with our hypothesis that much of the freshwater and organic material found in the coastal surface waters was transported by the Sagavanirktok and Kuparuk Rivers. In 2019, the fit between DOC and $a_g(440)$ was poor ($r^2 = 0.00056$). This lack of correlation may relate to failures in the filter system allowing large particles (greater than 0.2 μm in diameter) into the measurement tube or increased presence of small mineral particles which enhanced scattering errors in the absorption measurement. These measurement artifacts could explain why values of $a_g(440)$ increase for some stations in 2019 despite similar concentrations of DOC (Fig. 2b).

Commonly used spectral slope ranges of the dissolved absorption coefficient are from 275 – 295 nm and 350 – 400 nm due to their direct correlation with molecular weight (Helms et al., 2008) and efficacy as a tracer for terrigenous dissolved organic material in river fed coastal margins (Fichot et al., 2012). The spectral slope from 412 to 550 and the concentration of DOC were found to correlate well ($r^2 = 70$) across both years of the current study. This relationship shows an increase in DOC concentration with a steepening of spectral slope, further supporting the notion that terrigenous organic material transported by rivers is dominating these coastal surface waters.

In this study, the backscattering coefficient of 470 nm, 532 nm, and 660 nm is well-correlated with POC over both years ($r^2 = 0.90$, 0.71, and 0.59 for 470, 532, and 660 nm respectively). However, it is important to note that across each wavelength, the slope of the regression as well as the strength of the regression differed. The relationship between POC and backscatter of 470

nm (blue) and 532 nm (green) light is very similar suggesting that these particulate assemblages backscatter 470 nm and 532 nm light to a nearly equal extent. The maximum value measurable by the $b_b(532)$ channel in the instrument used (WETLabs VSF3) was lower than the maximum value in the $b_b(470)$ channel, thus limiting its utility for estimating POC concentration in environments with high concentrations of particulates using an instrument with fixed detector gain. This discrepancy is also likely the reason why the correlation between POC and $b_b(470)$ is improved over the others. The relationship between POC and $b_b(660)$ is the worst, but also had the most measurements reach the detector maximum, and thus the smallest sample size. Generally though, improvements in statistical metrics for model accuracy are small for regression models to estimate POC from $b_b(470)$ compared with $b_b(660)$ (e.g., MdAPD of 25.2% vs. 28.9%).

One final important consideration is that there are substantial limitations to estimating POC from backscatter by particles alone, especially across environments where the characteristics of suspended particulate matter may vary. Our data represent a fairly homogenous assemblage of particulate materials thus the relationships appear fairly good. However, large variations in the relationship between POC and backscatter exist in other studies indicating the importance of understanding the particle composition when deriving these relationships (Koestner et al., 2022; Reynolds et al., 2016; Stramski et al., 1999). Koestner et al. (2021) indicates that while some mineral-dominated samples exhibit strong correlations between POC and optical backscatter, organic-dominated particle assemblages deviate greatly from said trends. While most of the particulates from Stefansson Sound fall in the mineral dominated category (Koestner et al., 2021), it is possible that during periods of high riverine discharge, such as the spring freshet, the

510 bulk composition shifts more towards organic particulate matter as POC and PON are both
511 elevated during this event (McClelland et al., 2014).
512
513 **4.2 Physical controls on the distribution of organic material within the coastal margin**
514 Our observations suggest that the vertical structure of water column properties within Stefansson
515 Sound is determined by the wind direction, riverine discharge, and river mouth proximity.
516 During periods of westerly winds and relatively high preceding precipitation, multiple density
517 strata are visible within the water column. These strata range from 1002 kg m^{-3} at the surface to
518 1020 kg m^{-3} at depths of 5 m and below. The density profiles indicate the presence of a
519 freshwater film at the top, a mixed layer in the middle, and an oceanic layer near the bottom. In
520 2018, the western most stations, K1 and S1, have more defined stratification between the layers
521 while stratification is much weaker at the eastern stations, N1 and KAD1. This is likely due to
522 the proximity of these stations to the river mouths where the plume is still thin, while the western
523 stations are further from the source and more mixing and settling has occurred at these stations.
524 Further, the mixing in 2018 is likely buoyancy driven as the weak westerly winds perturb the
525 flow of the river plume less and facilitate calmer waters. This is also visible in the backscatter
526 profiles as N1 and KAD1 have higher baseline backscatter than K1 and S1 (**Fig 4).** The 2019
527 density profiles suggest an overall more saline and well-mixed environment. The western
528 stations, K1, KS1, and S1 have a thin slightly fresh surface layer with a near oceanic bottom
529 layer. Again, this is likely due to the proximity to the mouths of the rivers which constantly
530 inject some amount freshwater regardless of upstream precipitation**.** The more offshore stations,
531 S2 and UPE80, have a deeper mixed layer, with the deeper layer starting at ~8 m at S2 and ~19
532 m at UPE80.

Heavy rainfall preceding the 2018 sample period significantly increased riverine discharge and is a likely explanation for the significantly higher (unpaired *t*-test, $p < 0.05$) surface concentrations of DOC compared to what was measured during the 2019 sample period, which was preceded by much less rainfall. This is supported by the strong correlation between DOC and salinity ($r^2 = 0.97$), which indicates that fresher water contains higher concentrations of organic material in this region. However, an additional complexity to this system is that rivers are not the sole source of freshwater to the coastal margin. In 2018, sea-ice persisted in the coastal waters throughout the summer and fall which is much longer into the year than usual. As this ice melted, it created a secondary source of freshwater and organic material that could potentially resemble riverine sources with the methods used in this study (Underwood et al., 2019). An ice floe was directly on top of the K1 station in 2018 which had to be moved to access a mooring below. This melting floe along with surrounding melting floes resulted in multiple defined strata with different temperature-salinity characteristics than were measured in surface waters at other stations within the same year (**Fig. 5)**. This is also seen in the density profiles (**Fig. 4)**. Satellite imagery from Landsat, Sentinel, and MODIS suggests that the prevailing sea-ice is likely not from the landfast region but instead broken off from the Arctic icepack and drifted shoreward. Thus, while the salinity correlation with DOC appears robust, when examining this relationship in future studies it is important to consider that events like this may occur with less frequency as the Arctic climate warms. Further, the DOC supplied by this source may be of differing chemical character and/or bioavailability which may warrant a more specified study within this region.

4.3 Implications to satellite remote sensing of Arctic coastal waters

556 The type of *in situ* field-work described in this study offers insight into the optical relationships
557 and spatial distributions of organic material in Arctic coastal margins, but is ultimately spatially
558 and temporally limited. Remote sensing techniques offer a valuable future avenue for filling in
559 our understanding of biogeochemical cycling over space and time in this region. This study
560 provides a quantitative view into the base variables of the remote sensing reflectance which is
561 proportional to the sum of all backscattering constituents over the sum of all absorbing
562 constituents within surface waters. Here we provide near surface measurements of commonly
563 used optical proxies for these variables. Moreover, we relate these proxies to biogeochemical
564 parameters DOC and POC; these relationships can aid in the construction of quasi-analytical and
565 inverse algorithms designed to estimate quantities and qualities of surface organic material from
566 orbital and sub-orbital platforms (Lee et al., 2002; Loisel et al., 2000; Maritorena et al., 2002). In
567 addition to providing the required infrastructure to evaluate the organic carbon dynamics in these
568 coastal margins over longer timespans, these proxies also show that studying these systems on
569 finer spatial resolutions may best be done using satellite algorithms. While Arctic coastal
570 margins are optically complex, they are also optically variable with large dynamic ranges in
571 absorption and backscatter as seen in this study. These dynamics are easily identified by multi-
572 and hyper- spectral satellites. Hyper spectral satellites offer the extended capability to examine
573 pixel-scale spectral shapes that may provide the ability to differentiate groups of organic matter
574 within the bulk DOC pool. Further Arctic coastal margins experience extreme seasonality with
575 respect to not only rainfall as discussed in this study, but also landfast ice and sea-ice during the
576 rest of the year. Field studies have the potential to miss keystone events and misrepresent the
577 greater picture in the region while satellite methods offer the unique capability for repeat studies
578 throughout the sunlit parts of the year.

579

580 **4.4 Complexities and future work**

581 Beyond applications to remote sensing, this study opens many doors for future research within
582 Arctic coastal margins. We revealed that using standard optical proxies leaves some DOC
583 unaccounted for within this system. This is suggested by the non-zero y-intercept of the
584 relationship between fDOM and DOC (**Fig. 2**). To fully quantify the DOC concentration in the
585 coastal Arctic, we suggest the utilization of multiple fluorescent pairings to account for the entire
586 dissolved organic carbon pool. Fluorescent peak ratios reveal further insight into the DOC pool
587 in addition to concentration. The ratio of peak T (270/ 340 nm) to peak A (260/ 380-460 nm)
588 (T/A) describes the relative contribution of protein fluorescence relative to that of terrestrial
589 humic material. The ratio of peak M (290-310/370-410 nm) to peak C (350/ 420-480 nm) (M/C)
590 indicates the relative contributions of microbially derived to terrestrially originated DOM
591 (Stedmon et al., 2014).

592

593 Finally, this study revealed the complexity of this system and that these small coastal margins are
594 not simply miniature versions of the larger six Arctic coastal systems commonly studied. Each
595 year showed similarities in hydrographic controls by the rivers, however each year also displayed
596 differences in the optical correlations with dissolved organic material, as well as variability in
597 vertical structure between measured variables. These differences warrant caution when using
598 data sets from any single study or any single year in the development of remote or autonomous
599 sensing platforms based on *in situ* data. This research highlights the interdisciplinarity required
600 to examine these Arctic coastal estuaries as they are dynamic systems with overlapping physical
601 drivers. Moreover, Arctic systems have the added complexities of ice dynamics as well as input

602 from terrestrial sources highly susceptible to larger scale meteorological forcing. The Arctic
603 Ocean is in a transition period that is introducing unprecedented environmental anomalies such
604 as increased warming and precipitation (Bintanja et al., 2017). This fragile ecosystem will be one
605 of the first to show rapid changes that could alter its role in the global carbon cycle. Spring
606 freshets may become more extreme and the ice-free season may extend further into the fall,
607 substantially increasing the total amount of organic material delivered by these affected rivers
608 (Bintanja et al., 2014). With the anticipated longer ice-free seasons and more precipitation, the
609 coastal margins will feel the impact of these changes just as strongly as the terrestrial regions.
610
611 Optical proxies can help increase the temporal and spatial understanding of DOC dynamics in
612 Arctic coastal margins allowing for the study of future changes to these important buffer
613 systems. We show that simple optical measurements such as $a_g(440)$, $S_{412\text{-}550}$, fDOM, and b_b
614 which can be measured *in situ,* reveal insight into the areal and vertical structure of organic
615 variables in Stefansson Sound. This research offers preliminary insight into some of the topics of
616 interest of ongoing research projects investigating the adjacent lagoons and estuaries, as well as
617 the efficacy and utility of optical proxies in inshore and offshore remote applications. More
618 importantly, this research identifies regions of uncertainty in studying complex systems such as
619 Alaskan Arctic coastal margins. Specifically, in this study we've identified that fluorometers are
620 often best used in pairs when representing DOC, and optical backscatter at different wavelengths
621 exhibit varying relationships with POC concentrations.
622
623 Future directions for this research include improving the understanding of temporal patterns in
624 this region with respect to organic matter delivery and distribution. Specifically, studying the

source distribution during extreme events such as the spring freshet, or longer endured events such as the early spring ice melt. Studying the organic material found in the rivers during the spring freshet with spectral fluorescence and methodologies specialized in understanding the bioavailability will provide valuable understanding to the river endmember before it is transformed and transported within the coastal margins.

Acknowledgements

This research was funded by the National Aeronautics and Space Administration's Carbon Cycle and Ecosystems (CCE) program (award NNX17AI72G). The field work in this study was approved under permit from the North Slope Borough (DPCS #18-433). We thank the environmental representatives at British Petroleum Exploration Alaska for facilitating access to the field sites via their lease area. We give special thanks to Captain Mike Fleming (R/V *Ukpik*) for his expertise and guidance in our open water deployment and profiles. Further, we acknowledge and thank Gretchen Swarr for aiding in pre-cruise preparation and post-cruise sample analysis, and Dariusz Stramski for offering his expertise within the analysis of the relationships between optical backscatter and particulate organic carbon.

Data Repository

Data from this project are stored on NASA's SeaBass public access database under the experiment Prudhoe_Freshets. DOI for access to these data is 10.5067/SeaBASS/PRUDHOE_FRESHETS/DATA001

References

Bintanja, R., & Andry, O. (2017). Towards a rain-dominated Arctic. *Nature Climate Change, 7*(4), 263-267. doi:10.1038/nclimate3240

Bintanja, R., & Selten, F. M. (2014). Future increases in Arctic precipitation linked to local evaporation and sea-ice retreat. *Nature, 509*(7501), 479-482. doi:10.1038/nature13259

Coble, P. G. (1996). Characterization of marine and terrestrial DOM in seawater using excitation-emission matrix spectroscopy. *Marine Chemistry, 51*(4), 325-346. doi:https://doi.org/10.1016/0304-4203(95)00062-3

EDCT. (2020). *Meteorological monitoring program at Toolik, Alaska*. Retrieved from: https://toolik.alaska.edu/edc/monitoring/abiotic/met-data-query.php

Fichot, C. G., & Benner, R. (2012). The spectral slope coefficient of chromophoric dissolved organic matter (S275–295) as a tracer of terrigenous dissolved organic carbon in river-influenced ocean margins. *Limnology and Oceanography, 57*(5), 1453-1466. doi:https://doi.org/10.4319/lo.2012.57.5.1453

Gonçalves-Araujo, R., Granskog, M. A., Bracher, A., Azetsu-Scott, K., Dodd, P. A., & Stedmon, C. A. (2016). Using fluorescent dissolved organic matter to trace and distinguish the origin of Arctic surface waters. *Scientific Reports, 6*(1), 33978. doi:10.1038/srep33978

Helms, J. R., Stubbins, A., Ritchie, J. D., Minor, E. C., Kieber, D. J., & Mopper, K. (2008). Absorption spectral slopes and slope ratios as indicators of molecular weight, source, and photobleaching of chromophoric dissolved organic matter. *Limnology and Oceanography, 53*(3), 955-969. doi:https://doi.org/10.4319/lo.2008.53.3.0955

Howell, S., Brady, M., Derksen, C., & Kelly, R. (2016). Recent changes in sea ice area flux through the Beaufort Sea during the summer. *Journal of Geophysical Research: Oceans, 121*, n/a-n/a. doi:10.1002/2015JC011464

Koestner, D., Stramski, D., & Reynolds, R. A. (2021). Characterization of suspended particulate matter in contrasting coastal marine environments with angle-resolved polarized light scattering measurements. *Applied optics, 60*(36), 11161-11179. doi:10.1364/AO.441226

Koestner, D., Stramski, D., & Reynolds, R. A. (2022). A Multivariable Empirical Algorithm for Estimating Particulate Organic Carbon Concentration in Marine Environments From Optical Backscattering and Chlorophyll-a Measurements. *Frontiers in Marine Science, 9*. doi:10.3389/fmars.2022.941950

Laney, S. R., & Okkonen, S. (2022). An autonomous buoy system for observing spring freshet plumes under landfast sea ice. *Limnology and Oceanography: Methods, 20*(1), 15-25. doi:https://doi.org/10.1002/lom3.10472

Lee, Z., Carder, K. L., & Arnone, R. A. (2002). Deriving inherent optical properties from water color: a multiband quasi-analytical algorithm for optically deep waters. *Applied optics, 41*(27), 5755-5772. doi:10.1364/AO.41.005755

Loisel, H., & Stramski, D. (2000). Estimation of the Inherent Optical Properties of Natural Waters from the Irradiance Attenuation Coefficient and Reflectance in the Presence of Raman Scattering. *Applied optics, 39*, 3001-3011. doi:10.1364/AO.39.003001

Mann, P. J., Spencer, R. G. M., Hernes, P. J., Six, J., Aiken, G. R., Tank, S. E., . . . Holmes, R. M. (2016). Pan-Arctic Trends in Terrestrial Dissolved Organic Matter from Optical Measurements. *Frontiers in Earth Science, 4*(25). doi:10.3389/feart.2016.00025

Maritorena, S., Siegel, D. A., & Peterson, A. R. (2002). Optimization of a semianalytical ocean color model for global-scale applications. *Applied optics, 41*(15), 2705-2714. doi:10.1364/AO.41.002705

Matsuoka, A., Bricaud, A., Benner, R., Para, J., Sempéré, R., Prieur, L., . . . Babin, M. (2012). Tracing the transport of colored dissolved organic matter in water masses of the Southern Beaufort Sea: relationship with hydrographic characteristics. *Biogeosciences, 9*(3), 925-940. doi:10.5194/bg-9-925-2012

Matsuoka, A., Hill, V., Huot, Y., Babin, M., & Bricaud, A. (2011). Seasonal variability in the light absorption properties of western Arctic waters: Parameterization of the individual components of absorption for ocean color applications. *Journal of Geophysical Research: Oceans, 116*(C2). doi:https://doi.org/10.1029/2009JC005594

McClelland, J. W., Townsend-Small, A., Holmes, R. M., Pan, F., Stieglitz, M., Khosh, M., & Peterson, B. J. (2014). River export of nutrients and organic matter from the North Slope of Alaska to the Beaufort Sea. *Water Resources Research, 50*(2), 1823-1839. doi:https://doi.org/10.1002/2013WR014722

Novak, M. G., Cetinić, I., Chaves, J. E., & Mannino, A. (2018). The adsorption of dissolved organic carbon onto glass fiber filters and its effect on the measurement of particulate organic carbon: A laboratory and modeling exercise. *Limnology and Oceanography: Methods, 16*(6), 356-366. doi:https://doi.org/10.1002/lom3.10248

Osburn, C. L., Boyd, T. J., Montgomery, M. T., Bianchi, T. S., Coffin, R. B., & Paerl, H. W. (2016). Optical Proxies for Terrestrial Dissolved Organic Matter in Estuaries and Coastal Waters. *Frontiers in Marine Science, 2*(127). doi:10.3389/fmars.2015.00127

Parsons, T. R., Maita, Y., & Lalli, C. M. (1984). A Manual of Chemical and Biological Methods for Seawater Analysis.). Retrieved from https://www.cambridge.org/core/article/t-r-parsons-y-maita-c-m-lalli-1984-a-manual-of-chemical-and-biological-methods-for-seawater-analysis-xiv-173-pp-oxford-pergamon-press-price-550-us-895-flexicover-isbn-0-08-030288-2-hard-cover-0-08-030287-4-flexicover/D6B472FF1C39AD26EFB9085425EE57E5

Reynolds, R. A., Stramski, D., & Neukermans, G. (2016). Optical backscattering by particles in Arctic seawater and relationships to particle mass concentration, size distribution, and bulk composition. *Limnology and Oceanography, 61*(5), 1869-1890. doi:https://doi.org/10.1002/lno.10341

Spencer, R. G. M., Butler, K. D., & Aiken, G. R. (2012). Dissolved organic carbon and chromophoric dissolved organic matter properties of rivers in the USA. *Journal of Geophysical Research: Biogeosciences, 117*(G3). doi:https://doi.org/10.1029/2011JG001928

Stedmon, C., & Cory, R. (2014). Biological origins and fate of fluorescent dissolved organic matter. *Aquatic Organic Matter Fluorescence*.

Stedmon, C. A., Amon, R. M. W., Rinehart, A. J., & Walker, S. A. (2011). The supply and characteristics of colored dissolved organic matter (CDOM) in the Arctic Ocean: Pan Arctic trends and differences. *Marine Chemistry, 124*(1), 108-118. doi:https://doi.org/10.1016/j.marchem.2010.12.007

Stramski, D., Reynolds, R. A., Kahru, M., & Mitchell, B. G. (1999). Estimation of Particulate Organic Carbon in the Ocean from Satellite Remote Sensing. *Science, 285*(5425), 239-242. doi:10.1126/science.285.5425.239

747 Sullivan, J. M., Twardowski, M. S., Zaneveld, J. R. V., Moore, C. M., Barnard, A. H.,
748 Donaghay, P. L., & Rhoades, B. (2006). Hyperspectral temperature and salt dependencies
749 of absorption by water and heavy water in the 400-750 nm spectral range. *Applied optics,*
750 *45*(21), 5294-5309. doi:10.1364/AO.45.005294
751 Underwood, G. J. C., Michel, C., Meisterhans, G., Niemi, A., Belzile, C., Witt, M., . . . Koch, B.
752 P. (2019). Organic matter from Arctic sea-ice loss alters bacterial community structure
753 and function. *Nature Climate Change, 9*(2), 170-176. doi:10.1038/s41558-018-0391-7
754 Walker, S. A., Amon, R. M. W., & Stedmon, C. A. (2013). Variations in high-latitude riverine
755 fluorescent dissolved organic matter: A comparison of large Arctic rivers. *Journal of*
756 *Geophysical Research: Biogeosciences, 118*(4), 1689-1702.
757 doi:https://doi.org/10.1002/2013JG002320
758 Ward, C. P., & Cory, R. M. (2015). Chemical composition of dissolved organic matter draining
759 permafrost soils. *Geochimica et Cosmochimica Acta, 167*, 63-79.
760 doi:https://doi.org/10.1016/j.gca.2015.07.001
761 Weingartner, T., & Okkonen, S. R. (2001). *Beaufort Sea Nearshore Under-Ice Currents:*
762 *Science, Analysis and Logistics*.
763 Weishaar, J. L., Aiken, G. R., Bergamaschi, B. A., Fram, M. S., Fujii, R., & Mopper, K. (2003).
764 Evaluation of Specific Ultraviolet Absorbance as an Indicator of the Chemical
765 Composition and Reactivity of Dissolved Organic Carbon. *Environmental Science &*
766 *Technology, 37*(20), 4702-4708. doi:10.1021/es030360x
767 Youcha, E. K., Gieck, R. E., Arp, C. D., Stuefer, S., & Irving, K. (2015). *Standard Operating*
768 *Procedure and Workplan for the Terrestrial Environmental Observation Network*
769 *(TEON) – Arctic Landscape Conservation Cooperative: Kuparuk River Basin and*
770 *Adjacent Catchments*. Retrieved from http://hdl.handle.net/11122/10389
771

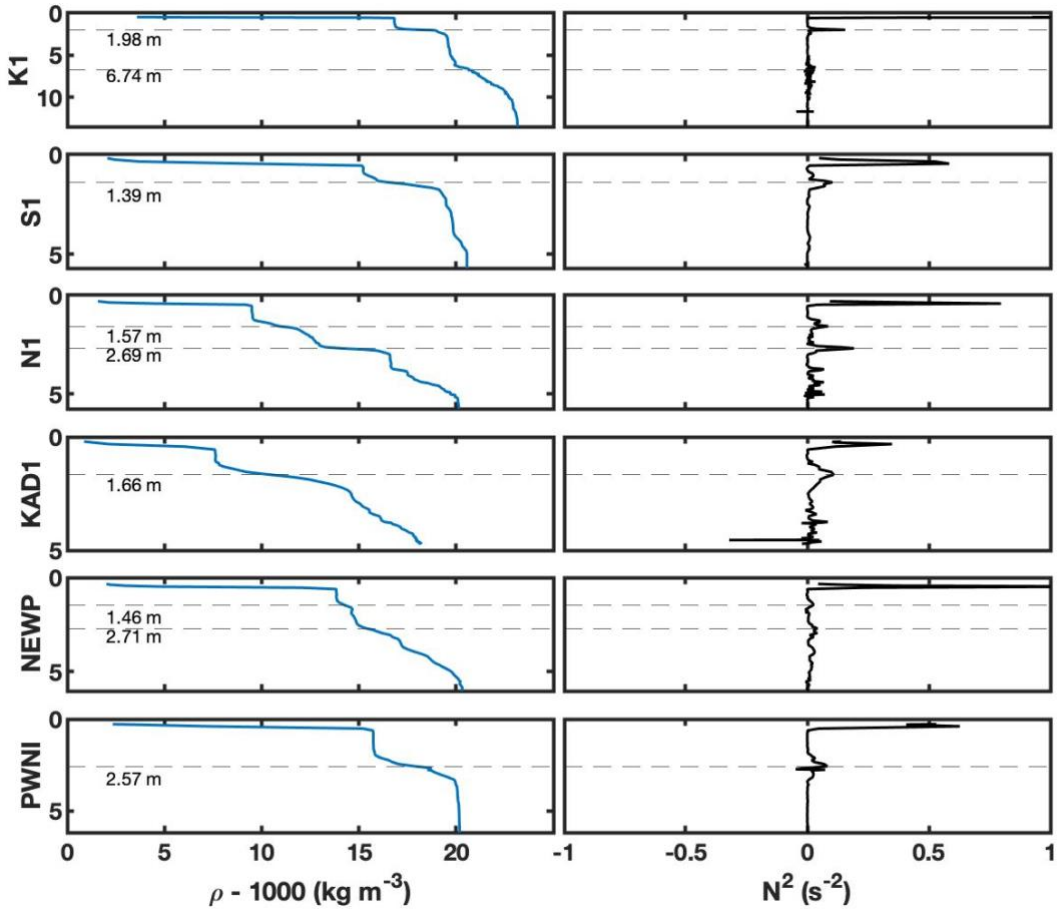

Figure S1. 2018 Density profiles (left) shown alongside Brunt-Vaisala frequency (right). Dashed lines indicate potential mixed layer depths according to largest Brunt-Vaisala peak below the freshwater film (~ 2m).

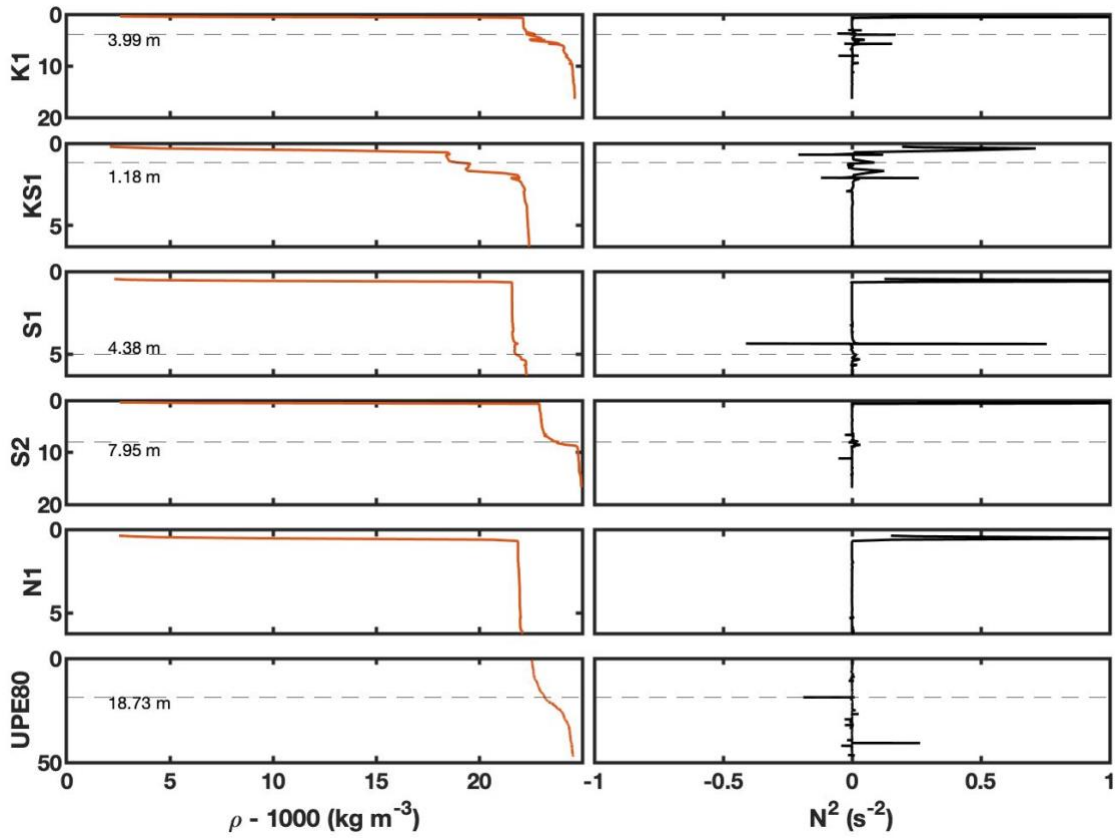

Figure S2. 2019 Density profiles (left) shown alongside Brunt-Vaisala frequency (right). Dashed lines indicate potential mixed layer depths according to largest Brunt-Vaisala peak below the freshwater film (~ 2m).

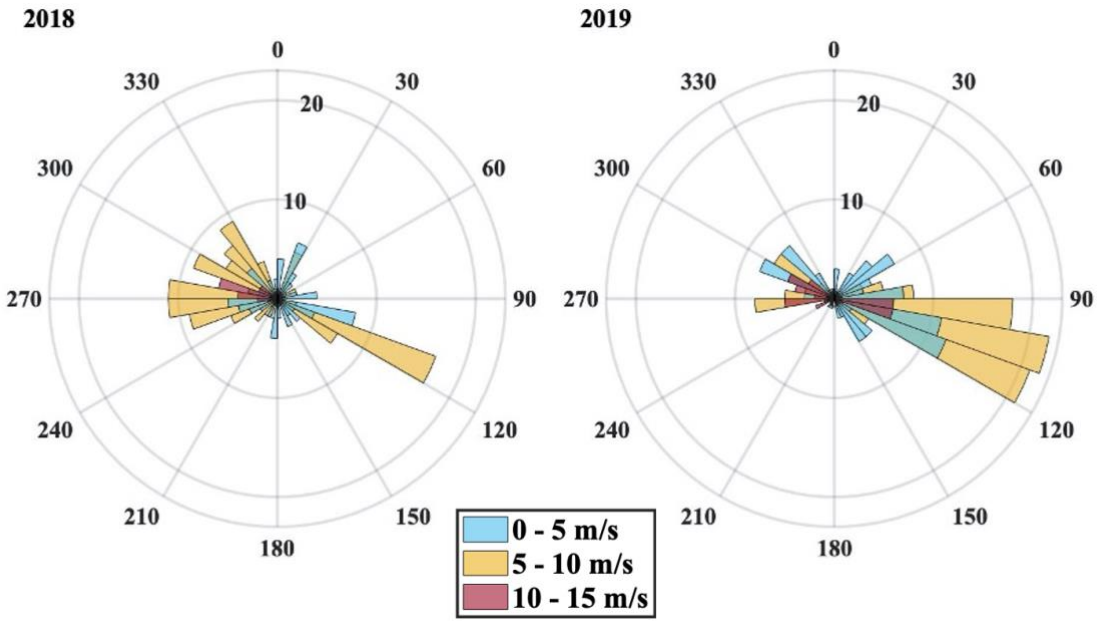

Figure S3. Wind direction histogram during 1 – 10 September 2018 (left) and 4 – 13 August, 2019 (right). Radial values depict wind speed in units of m/s, polar values depict wind direction.